Generalization of the Wall Panel Theory Applied to Structural Cores C and Double T

Weslley Imperiano Gomes de Melo[1], Normando Perazzo Barbosa[2]

Abstract— **This paper presents the Generalization of Wall Panel Theory (GWPT), placing the walls that make up the column in a structural core shape with an angulation different from orthogonality. As for the geometry of the structural core C and double T, the inclination analysis of the walls is performed in order to diminish the sheer forces for the effective structural launching for columns, seeking to minimize the stresses with the mere change of the wall inclination. Finally, we use the particular case of double T core with walls orthogonal to each other and validate the generalized formulations in this article, concluding the total resumption of the values of sectoral ordinates. In addition, the first three modes of vibration of the C cores and double T are used, in conclusion, 95.89 % and 95.81 % of convergence between the values obtained via CMT and FEM, respectively.**

Keywords— **Wall Panel Theory (WPT), Generalization (GWPT), Continuous Medium Technique (CMT), Sectoral Inertia and Optimal Positioning of Wall**

I. INTRODUCTION

The cross sections of the tall columns (also called slender columns, and, for example, the bridge columns are mentioned) become economically viable if adopted with hollow section and thin walls. In cases of asymmetric sections, the combined effect of flexure and torsion is activated due to non-coincidence of the centers of gravity (CG) and torsion (D).

The determination of the thin-walled cross-sectional properties, such as the placement of the torsion center and the sectoral inertia I_ω, is formulated in Vlassov (1962). However, in determining the absolute sectoral ordinate diagram ω_{pc} and the resulting sectoral inertia, although Vlassov presents the integral formulation, in the specific literature there are only applications in sections with curved or orthogonal walls between each other. Still, in the aforementioned work, there is an exemplification of the walls with distinctive inclination of the orthogonality between the panels, however in numerical exercises and without the proper generalized trigonometric formulation. In short, for Vlassov (1962, p. 194 and 200) the analysis of inclined walls is performed in numerical exercises.

And it is because of this shortcoming that, in this paper, the generalization of the wall panel theory (GWPT) presented in

Barbosa (1978) will be formulated. Vlassov's notation will be adopted and extended via generalized trigonometric equation, thus formulating the GWPT.

Years later, in Murray (1986, p. 54 - 192), Kollbrunner and Basler (1969), and Campanari (1985, v. 2, p. 723 - 749) the theory of thin walls postulated by Vlassov (1962) is recovered, however, with new (purely numerical) examples for inclined thin walls, always through input data, and without proper postulation of the generalized trigonometric formulation. Given the analysis of the overall stability of structural cores, Zalka (2000, p. 121 - 153 and 238 - 277) stands out. However, in both publications, the equation is formulated only for orthogonal walls between each other.

For the structural core columns, and under the approach of the formation of wall panels, consisting of sheet metal, there is the coincidence of the placement of the center of gravity (CG) and the center of mass (CM), which originates from the homogeneity of the mechanical properties (which is due to the steel machining process). See such placement in Figure 1 (a). In the case of reinforced concrete columns, the location of the CG of the raw section with the CM is not coincident. Therefore, the transformation of the coordinates from the CM to CG will be necessary (see Figure 1 c). After such coordinate transformation, the dynamic formulation of the column is composed of a reinforced concrete structural core, together with the static portion of the wall panel theory referenced in the center of gravity of the cross section. See Figure 1 (b).
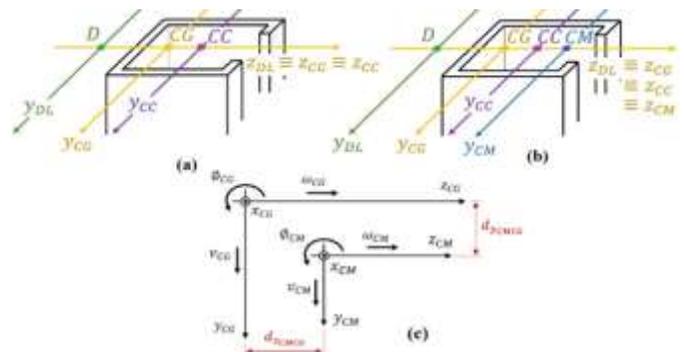
Fig. 1. Geometric Center Distribution: (a) for metal section; (b) for reinforced concrete column; and (c) coordinate transformation from the CM to the CG of the reinforced concrete section.

[1]Doctor in Structures and Materials, Professor of Civil Engineering at UFRPE, Recife, Pernambuco, Brazil. E-mail: weslleyimperiano@hotmail.com; weslley.gomes@ufrpe.br
[2]Doctor in Structures, UFPB Full Professor in Structures and Materials, João Pessoa, Paraíba, Brazil. E-mail: nperazzob@yahoo.com.br.

The formulation of the wall panels is initially presented in Mancini (1972) with a single structural element (see Figure 1 a). In Barbosa (1978), Tso (1983) and Smith and Taranath (1972), the structural cores are solved via flexure-torsion theory and subdivided into wall panels. In such scientific works, the wall panel theory (WPT) is formulated, starting from an open cross section column and orthogonal thin walls, being partially braced by lintels (with length L_L and spaced from axis to axis from distance h). The structural core shape, studied by researchers in the 1970s and 1980s, is characterized by five walls numbered from (1) to (5) and with four intersections. As presented in Laier (1984) and Laredo (1977), the dynamic analysis of the structures is conveniently processed via the continuous technique, basically consisting in considering the stiffness of the horizontal connecting elements (slabs and beams) through properties and stresses distributed at the height of the column. In addition, in the mentioned work of 1984, the analysis of the wall vibration is processed, recommending the beginning of the contributions of the continuous medium technique (CMT) applied to dynamic problems. In this paper we will use the dynamic formulation of CMT in generalized inclination thin-walled bridge columns, see Melo & Barbosa (2020 a,b).

The use of continuous technique over discrete models, such as the finite element method (BREBRIA; FERRANTE, 1975) and Dhatt et al. (2005), finite difference method (GUELFOND, 1963), boundary element method among others, is motivated by simplification of processing (consequence of the reduced number of parameters involved). The number of parameters via discrete finite element analysis is a function of the discretization mesh and how far-fetched and refined the mesh needs to be. In the search for displacements, rotations and stresses, the use of more complex interpolating functions or the refinement of the mentioned mesh is necessary.

In the dynamic modeling of vertical panels via the continuous medium technique, Stamato (1980); Laier (1984) and Simith and Coull (1991) reiterate that the column locking occurs horizontally along the height. Thus, the slabs or simply the deck (in the case of bridges) are employed as elements of infinite stiffness in their planes and the transverse stiffness of such elements is neglected. In order to justify the simplification of the structural operation of horizontal locks as diaphragms, Biggs (1964) is cited and the fact that magnitudes of horizontal movements are much larger than those observed in the vertical direction is reinforced, and, therefore, the latter is discarded.

II. WALL PANEL THEORY

A. Geometric Properties of Thin-Walled Cross-Section under Generalized Structural Core Form

The generalization of the wall panel theory will be processed in this paper item by imposing generic inclination for all the walls that make up the structural core. The notation adopted for the placement of the centroidal axes $\left(y \equiv y_{CG}, z \equiv z_{CG}\right)$ and the auxiliary $\left(x^*, y^*\right)$ axes is presented in Figure 2.

From the provisional point P located at the intersection of

wall panels (1) and (3), as shown in figure 2, the diagramming of the sectoral ordinates ω_p with arbitrary pole P is made. For such, the convention defined in Vlassov (1962) and the vector area calculation between two vectors is used, concluding diagrammatically ω_p that which is presented in Figure 3. Where: $\Delta\omega_1 = \Delta\omega_3 = 0$; $\Delta\omega_2 = b_1 . b_2 . \sin(\theta_1 - \theta_2)$;

$\Delta\omega_4 = -b_1 . b_4 . \sin(\theta_1 + \theta_4) - b_2 . b_4 . \sin(\theta_2 + \theta_4)$ e

$\Delta\omega_5 = b_3 . b_5 . \sin(\theta_3 + \theta_5)$. And: b_i is the length at cross section of the ith wall panel, and θ_i is the angle of incidence of the wall i in relation to the auxiliary axis x^* originating from the provisional pole P.

By calculating the coordinates of the center of gravity (CG) of the cross section presented in Figure 2, the position of the CG is defined at the expense of the provisional pole P and the auxiliary axes x^* and y^*, as:

$$b_{CG_z} = \frac{b_1^* . \cos\theta_1 + b_2^* . \cos\theta_2 + b_3^* . \cos\theta_3 + b_4{}^2 . \cos\theta_4 + b_5{}^2 . \cos\theta_5}{2 . (b_1 + b_2 + b_3 + b_4 + b_5)} \quad (1\,a)$$

$$b_{CG_y} = \frac{b_1^* . \sin\theta_1 + b_2^* . \sin\theta_2 + b_3^* . \sin\theta_3 + b_4{}^2 . \sin\theta_4 + b_5{}^2 . \sin\theta_5}{2 . (b_1 + b_2 + b_3 + b_4 + b_5)} \quad (1\,b)$$
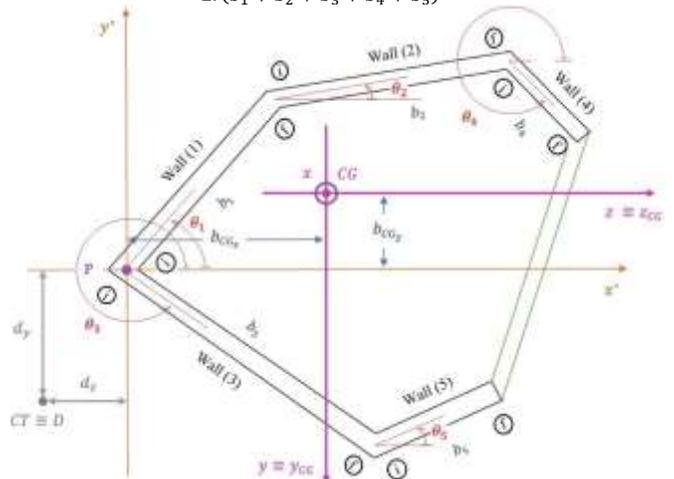
Fig. 2. Generalized placement of the walls in the structural core.
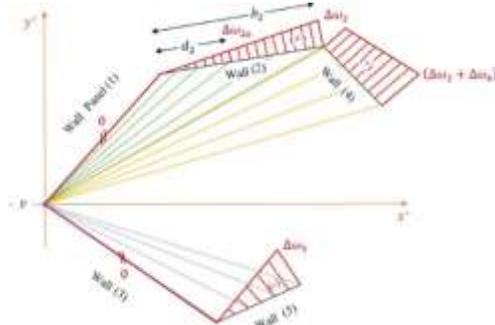
Fig. 3. Sectoral ordinate diagrams ω_p with temporary pole P.
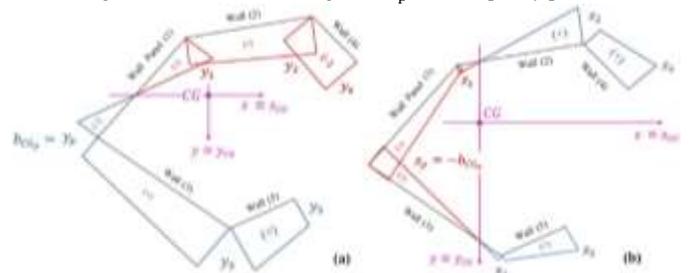
Fig. 4. Coordinate diagram for the inclined walls: (a) axis y and (b) axis z.

with: $b_1^* = b_1{}^2 + 2.b_1.b_2 + 2.b_1.b_4$; $b_2^* = b_1{}^2 + 2.b_2.b_4$; $b_3^* = b_3{}^2 + 2.b_3.b_5$. The coordinate diagrams y and z, of the structural core, are presented in Figure 4. Coordinates y_i and z_i of the final ends of the wall panels i, are expressed by: $z_1 = z_p + b_1.\cos\theta_1$; $z_2 = z_1 + b_2.\cos\theta_2$; $z_3 = z_p + b_3.\cos\theta_3$; $z_4 = z_2 + b_4.\cos\theta_4$; $z_5 = z_3 + b_5.\cos\theta_5$; $y_1 = y_p - b_1.\sin\theta_1$; $y_2 = y_1 - b_2.\sin\theta_2$; $y_3 = y_p - b_3.\sin\theta_3$; $y_4 = y_2 - b_4.\sin\theta_4$ and $y_5 = y_3 - b_5.\sin\theta_5$. With: $z_p = -b_{CG_z}$ e $y_p = b_{CG_y}$

Due to the integration of the coordinate diagrams y (see Figure 4a) and coordinates z (see Figure 4b) by the diagram ω_p shown in Figure 3, the placement of the torsional center D is concluded through the geometric interpretation, defining, thus, the position of the torsional center by the distances d_y and d_z and shown in Figure 2, resulting in:

$$d_y = \frac{t}{6.I_y}.\{\Delta\omega_{2a}.[-d_2.z_1 + (b_2 - d_2).z_2]$$
$$+ \Delta\omega_2.[z_2.(3.b_4 + 2.b_2 - 2.d_2) + 3.b_4.z_4]$$
$$+ \Delta\omega_4.(b_4.z_2 + 2.b_4.z_4)$$
$$- \Delta\omega_5.(b_5.z_3 + 2.b_5.z_5)\} \quad (2a)$$

$$d_z = \frac{t}{6.I_z}.\{\Delta\omega_2.[b_2.y_1 + y_2.(2.b_2 + 3.b_4) + 3.b_4.z_4]$$
$$+ \Delta\omega_4.(b_4.y_2 + 2.b_4.y_4)$$
$$+ \Delta\omega_5.(b_5.y_3 + 2.b_5.y_5)\} \quad (2b)$$

with: $\Delta\omega_{2a} = \frac{d_2}{b_2}.\Delta\omega_2$; $d_2 = \frac{|z_1|.b_2}{|z_1| + |z_2|}$; $I_z = \sum_{i=1}^{5}\{I_{z_i} + A_i.\Delta y_i{}^2\}$; $I_y = \sum_{i=1}^{5}\{I_{y_i} + A_i.\Delta z_i{}^2\}$; and: $\Delta y_i = |y_{CG_i}^* - b_{CG_y}|$; $\Delta y_i = |x_{CG_i}^* - b_{CG_z}|$; $I_{z_i} = \frac{I_{x_i}^{**} + I_{y_i}^{**}}{2} + \frac{I_{x_i}^{**} - I_{y_i}^{**}}{2}.\cos(2.\theta_i)$ and t is the thickness of the walls.

Finally, when drawing the absolute sectoral ordinate diagram ω_{pc} with a scanning pole at the torsional center D, as shown in Figure 5, pointing out that the torsional center D is the arbitrary position where, when transverse forces are applied, only flexure efforts are activated. It is also recalled that the moment of sectoral inertia I_ω equals the mechanical strength of the structural core to the combined action of flexure-torsion.
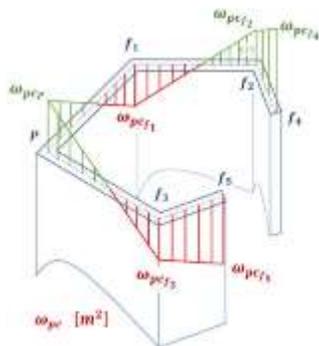
Fig. 5. Absolute coordinate diagram ω_{pc}, with scanning pole in the torsional center.

resulting by ordinates $\omega_{pc_{f_i}}$ at the end edges of the wall panels i, as follows:

$$\omega_{pc_{f_1}} = \omega_{pc_p} + \Delta\omega_{pc_{f_1}} \quad (3a)$$
$$\omega_{pc_{f_2}} = \omega_{pc_{f_1}} + \Delta\omega_{pc_{f_2}} \quad (3b)$$

$$\omega_{pc_{f_3}} = \omega_{pc_p} + \Delta\omega_{pc_{f_3}} \quad (3c)$$
$$\omega_{pc_{f_4}} = \omega_{pc_{f_2}} + \Delta\omega_{pc_{f_4}} \quad (3d)$$
$$\omega_{pc_{f_5}} = \omega_{pc_{f_3}} + \Delta\omega_{pc_{f_5}} \quad (3e)$$

with: $\omega_{pc_p} = d_y.d_z$; $\Delta\omega_{pc_{f_2}} = -b_2.(d_y.\cos\theta_2 - d_z.\sin\theta_2) + b_1.b_2.\sin(\theta_1 - \theta_2)$; $\Delta\omega_{pc_{f_1}} = b_1.(d_y.\cos\theta_1 - d_z.\sin\theta_1)$; $\Delta\omega_{pc_{f_3}} = -b_3.(d_y.\cos\theta_3 - d_z.\sin\theta_3)$; $\Delta\omega_{pc_{f_4}} = b_4.(d_y.\cos\theta_4 - d_z.\sin\theta_4) + b_1.b_4.\sin(\theta_1 - \theta_4) + b_2.b_4.\sin(\theta_2 - \theta_4)$ and $\Delta\omega_{pc_{f_5}} = b_5.(d_y.\cos\theta_5 - d_z.\sin\theta_5) + b_3.b_5.\sin(\theta_3 - \theta_5)$.

Through quadratic integration of the diagram ω_{pc} by the thickness t of the walls, the sectoral inertia $I_\omega = t.\int_s (\omega_{pc})^2 ds$ is expressed by:

$$I_\omega = \frac{b_1}{6}.\omega_{pc_p}.\left(2.\omega_{pc_p} + \omega_{pc_{f_1}}\right) + \frac{b_1}{6}.\omega_{pc_{f_1}}.\left(\omega_{pc_p} + 2.\omega_{pc_{f_1}}\right) +$$
$$+ \frac{b_2}{6}.\omega_{pc_{f_1}}.\left(2.\omega_{pc_{f_1}} + \omega_{pc_{f_2}}\right) + \frac{b_2}{6}.\omega_{pc_{f_2}}.\left(\omega_{pc_{f_1}} + 2.\omega_{pc_{f_2}}\right) +$$
$$+ \frac{b_3}{6}.\omega_{pc_p}.\left(2.\omega_{pc_p} + \omega_{pc_{f_3}}\right) + \frac{b_3}{6}.\omega_{pc_{f_3}}.\left(\omega_{pc_p} + 2.\omega_{pc_{f_3}}\right) +$$
$$+ \frac{b_4}{6}.\omega_{pc_{f_2}}.\left(2.\omega_{pc_{f_2}} + \omega_{pc_{f_4}}\right) + \frac{b_4}{6}.\omega_{pc_{f_4}}.\left(\omega_{pc_{f_2}} + 2.\omega_{pc_{f_4}}\right) +$$
$$+ \frac{b_5}{6}.\omega_{pc_{f_3}}.\left(2.\omega_{pc_{f_3}} + \omega_{pc_{f_5}}\right) + \frac{b_5}{6}.\omega_{pc_{f_5}}.\left(\omega_{pc_{f_3}} + 2.\omega_{pc_{f_5}}\right) \quad (4)$$

B. Geometric Properties of Thin-Walled Cross-Section under Generalized Structural double T form

Figure 6 shows the configuration of the cross section in double T with generalized positioning of the wall panels. The inclinations $\left(\theta_j\right)$ of the jth panel are also shown.
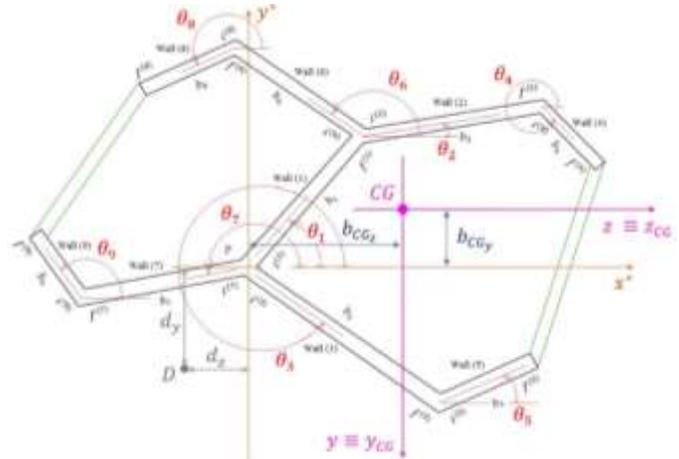
Fig. 6. Generalized placement of the walls in the structural core double T.

Aiming at the positioning of the torsional center D, the diagrams of provisional sectoral ordinates ω_p (see figure 7 a), the y coordinates of the jth panel (see figure 7 b), and the z coordinates (in figure 7 c) are drawn. The y and z coordinates of the wall panels are measured from the center of gravity of the cross section.
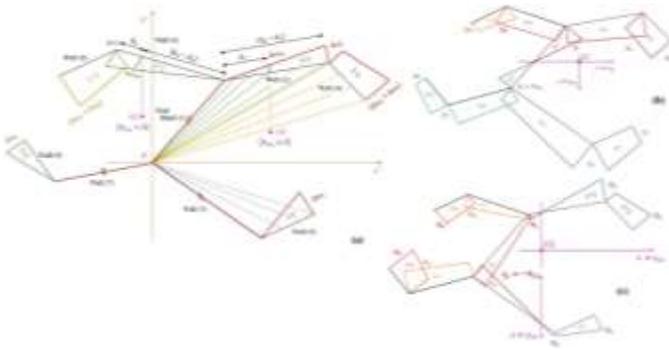
Fig. 7. Generalized double T column: (a) ω_p diagram, (b) y diagram and (c) z diagram.

Then, Figure 8 (a) shows the scan direction on the right C core, which composes the double T column, while Figure 8 (b) shows the positive scan on the left core. Figure 8 (c) shows the configuration of the absolute sectoral ordinate diagram ω_{pc}.
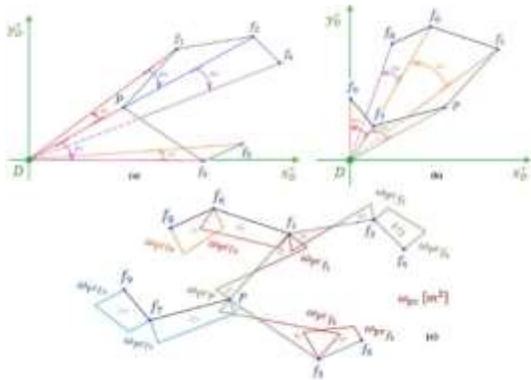
Fig. 8. Double T: scan on the right core (a), (b) on the left, and (c) ω_{pc} diagram.

In conclusion, the sectoral inertia I_ω , generalized in the sectoral ordinate diagram ω_{pc} (see Figure 8 c), is expressed as follows:

$$I_\omega \equiv t. \left\{ \frac{b_1}{6}.\omega_{pcP}.\Delta_{P1} + \frac{b_1}{6}.\omega_{pc_{f_1}}.\Delta_{1P} + \frac{b_2}{6}.\omega_{pc_{f_1}}.\Delta_{12} + \frac{b_2}{6}.\omega_{pc_{f_2}}.\Delta_{21} + \right.$$

$$+ \frac{b_3}{6}.\omega_{pcP}.\Delta_{P3} + \frac{b_3}{6}.\omega_{pc_{f_3}}.\Delta_{3P} + \frac{b_4}{6}.\omega_{pc_{f_2}}.\Delta_{24} + \frac{b_4}{6}.\omega_{pc_{f_4}}.\Delta_{42} +$$

$$+ \frac{b_5}{6}.\omega_{pc_{f_3}}.\Delta_{35} + \frac{b_5}{6}.\omega_{pc_{f_5}}.\Delta_{53} + \frac{b_6}{6}.\omega_{pc_{f_1}}.\Delta_{16} + \frac{b_6}{6}.\omega_{pc_{f_6}}.\Delta_{61} +$$

$$+ \frac{b_7}{6}.\omega_{pcP}.\Delta_{P7} + \frac{b_7}{6}.\omega_{pc_{f_7}}.\Delta_{7P} + \frac{b_8}{6}.\omega_{pc_{f_6}}.\Delta_{68} + \frac{b_8}{6}.\omega_{pc_{f_8}}.\Delta_{86} +$$

$$+ \frac{b_9}{6}.\omega_{pc_{f_7}}.\Delta_{79} + \frac{b_9}{6}.\omega_{pc_{f_9}}.\Delta_{97} \right\} \tag{5}$$

with the parameters of Equation (5) presented in the appendix.

The numerical validation of the sectoral ordinates required in Equation (4) is easily accomplished by adopting the sub-case of thin-walled double T column with wall panels orthogonal to each other, see Figure 9, resulting in: $\theta_1 = \theta_5 = \theta_9 = 90^0$, $\theta_6 = \theta_7 = 180^0$, $\theta_4 = \theta_8 = 270^0$, $\theta_2 = 0^0$, and $\theta_3 = 360^0$.
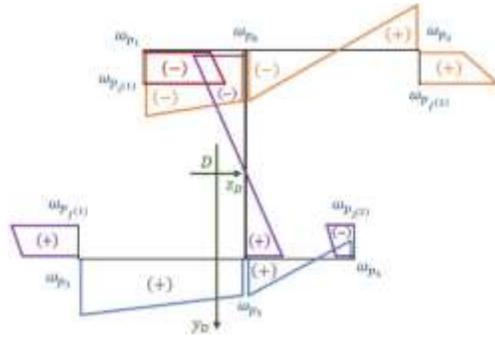
Fig. 9. Diagram of sectoral ordinates ω_{pc} for asymmetric double T section and with walls orthogonal to each other.

Thus, the main sectoral ordinate diagram ω_{pc} for the section without any symmetry is calculated by means of the geometric procedure previously defined, as well as in the determination of sectoral ordinate increments $\Delta\omega_{(i)}$ in the generic wall panel i, resulting in main sectoral ordinates, which fully reproduce the expressions in Vlassov (1962) and Kollbrunner & Basler (1969), as:

$$\omega_{p_1} = d_z.(d_y - b_4) - b_{1a}.(b_4 - d_y); \qquad \omega_{p_3} = d_y.(b_{7a} + d_z);$$

$$\omega_{p_2} = -d_z.(b_4 - d_y) + b_{1b}.(b_4 - d_y); \qquad \omega_{p_4} = d_y.(d_z - b_{7b});$$

$$\omega_{p_{i(1)}} = d_z.(d_y + b_3 - b_4) - b_{1a}.(b_3 + b_4 - d_y);$$

$$\omega_{p_{f(1)}} = d_z.(d_y - b_2) + b_{7a}.(b_2 + d_y); \qquad \omega_{p_5} = d_y.d_z;$$

$$\omega_{p_{i(2)}} = d_z.(d_y - b_5) - b_{7b}.(b_5 + d_y); \qquad \omega_{p_6} = -d_z.(b_4 - d_y);$$

$$\omega_{p_{f(2)}} = -d_z.(b_4 - b_6 - d_y) + b_{1b}.(b_4 - d_y).$$

III. STRUCTURAL CORE COLUMN MODELING

A. Contribution of Wall Panel inclination in structural laying of straight bridge columns

In order to exemplify the generalization carried out in item II (A) of this article, the variation of the sectoral inertia I_ω is used in detriment of the inclinations of wall panels (2) and (3), of which it is emphasized that the bimoment is directly proportional to the sectoral inertia (see more details in Flexural-Torsion Theory), reference by Mori and Munaiar Neto (2017) is made to this statement. The analysis is carried out for a straight bridge column, in which the bimoment and the resulting cross section flexure will be reduced by simply inclining the side walls (2) and (3). Tables 1 to 3 show sectoral inertia I_ω values to the detriment of the inclination variation θ_2 and θ_3. In such analysis, the inclinations presented in Figure 10 are considered.
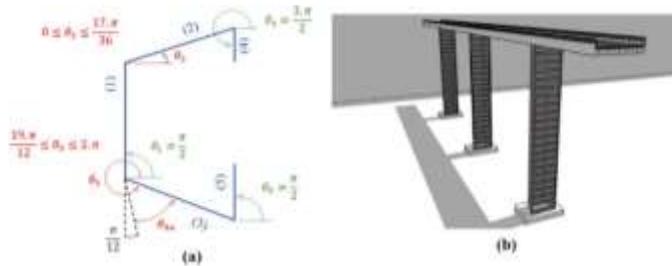
Fig. 10. Structural core geometry for analysis of the inclination variation of wall panels (2) and (3): (a) floor plan and (b) applicability in bridges with straight deck.

The sector inertia I_ω, see Equation (4), is dependent on the inclinations of the walls (1) to (5) of the structural core column. The configuration of such column is shown in Figure 9. However, it is convenient to adopt walls (1), (4), and (5) perpendicular to the bridge deck direction for straight bridges (see Figure 10 b). The structural engineer has the margin to project economic efficiency combined with the safety of the structure by inclining walls (2) and (3), thus seeking lesser internal forces (bimoment), deriving optimized resistant reinforcement bar (for the case of reinforced concrete column) and reduced thickness for the occurrence of metal columns.

Table 1 presents sectoral moments of inertia I_ω for the variation of the wall inclination (2) under the fixed positioning of the wall (3) in θ_3 of 285°. Tabulation is performed for three relative wall thicknesses, which are: $\eta_3 = {}^1/_{40}$ and $\eta_4 = 4$ presented as curve 1, the ratios $\eta_3 = {}^1/_{30}$ and $\eta_4 = 10$ for curve 2, and finally, in curve 3, $\eta_3 = {}^1/_{100}$ and $\eta_4 = 5$ is used.

TABLE I
VALUES OF I_ω $(x\,10^7)\,m^6$ FOR THE VARIATION OF THE INCLINATION OF WALLS (2) E (3) WITH θ_3 AND 285°

θ_2	curve 1	curve 2	curve 3
15⁰	0.639	0.361	53.103
30⁰	0.602	0.349	49.580
45⁰	0.509	0.298	41.449
60⁰	0.387	0.226	31.219
75⁰	0.222	0.127	17.886
85⁰	0.035	0.020	2.839

In this first analysis (Table I), the inclination of wall (3) is kept outdated 15° with respect to the skeleton axis of wall (1), to avoid functioning as a cutting wall, maintaining the three-dimensional configuration of the wall. Whereas, in Table II the same variation of the inclination of the wall panel (2) is carried out, but for θ_3 equal to 322.5°, and the average position in the variation range of the inclination is imposed to wall (3).

TABLE II
VALUES OF I_ω $(x\,10^7)\,m^6$ FOR THE VARIATION OF THE INCLINATION OF WALLS (2) E (3) WITH θ_3 AND 322,5°

θ_2	curve 1	curve 2	curve 3
15⁰	1.482	0.907	118.798
30⁰	1.542	0.931	123.598
45⁰	1.401	0.827	112.565
60⁰	0.934	0.539	75.494

75⁰	0.296	0.174	23.988
85⁰	0.036	0.034	2.786

Finally, Table III shows the variation of I_ω with the orthogonal fixation of wall (3) to wall (1), performing the variation of the wall panel inclination (2).

TABLE III
VALUES OF I_ω $(x\,10^7)\,m^6$ FOR THE VARIATION OF THE INCLINATION OF WALLS (2) E (3) WITH θ_3 AND 360°

θ_2	curve 1	curve 2	curve 3
15⁰	1,093	0,720	88,025
30⁰	1,309	0,827	104,988
45⁰	1,304	0,787	104,769
60⁰	0,913	0,532	73,671
75⁰	0,306	0,181	24,667
85⁰	0,037	0,040	2,771

Such analysis is aimed at allowing bridge designers to know which is the best angle to use in the inclination of these walls, contributing in this article item to straight bridges and to generate smaller bimoments (since I_ω is related to the bimoment by the thin wall section theory presented by Vlassov), adding economy to the project with the mere inclination of two of the walls that make up the structural core. Whereas, Figure 11 (a) presents the graph of the sectoral inertia variation I_ω with the modification of the wall inclination (2) and maintenance of the inclination of wall (3), and in relation 15° to wall (1). As wall (2) tends to approximate orthogonality $(\theta_2 = 0^o)$ with wall (1), sectoral inertia is increased. Hence, it is concluded that the structural core effect provides greater flexural torsion resistance, and it is also found that the greater the projection onto the floor plan of the thin-walled section, the greater the flexural torsion resistance.

Figure 11 (a) shows that the optimal of wall (2) occurs at 15^0 in relation to orthogonality with wall (1), when maintaining the minimum inclination of 15^0 between wall panels (1) and (3). Figures 10 (b) and 10 (c) analyze the variation of I_ω for the placement of wall (3) at 322.5^0 (half of the variation inclination range) and at 360^0 (orthogonal walls between each other). Even when imposing relative thicknesses with the ratios η_3 and η_4, the same occurrence is evidenced in Figure 16. Therefore, it can be concluded that the inclination of 30^0 in wall (2) is interesting when imposing the placement of wall (3) in the middle of the inclination range (in the case at 322.5^0).
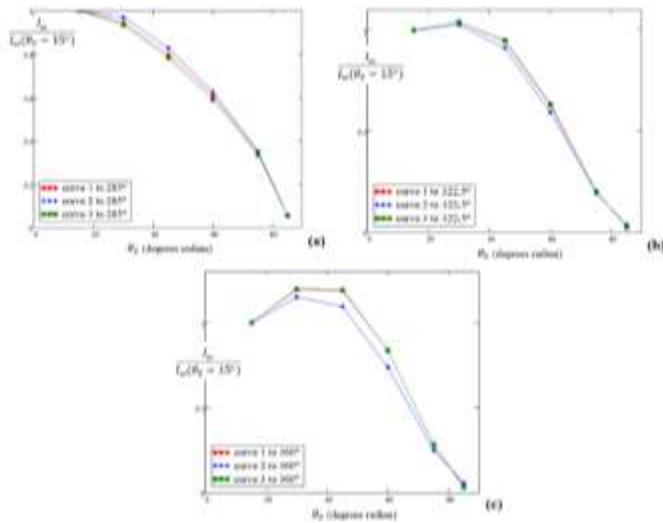
Fig. 11. variation chart from I_ω to θ_3: (a) 285^0, (b) 322.5^0 and (c) 360^0.

Fig. 12. Double T column: (a) analyzed geometry; variation chart of I_ω to (b) $\theta_3 = 285^o$ and $\theta_7 = 195^o$; (c) $\theta_3 = 322.5^o$ and $\theta_7 = 217.5^o$; and (d) $\theta_3 = 360^o$ and $\theta_7 = 180^o$.

In both analysis scenarios the following relations were adopted for the walls: $b_1 = b_2 = b_3$, $b_4 = b_5$, $t = b_1.\eta_3$ and $b_4 = \eta_4.t$.

B. Contribution of Wall Panel inclination in structural core double T

Similar to the procedure in item III (A), we now proceed to analyze the variation of the sectoral inertia I_ω for the double T column. Thus, Figure 12 (a) shows the geometry of the symmetrical section in double T, with the indications of the inclinations of the wall panels, whereas, in Table IV, the sectoral inertia values I_ω are presented to the detriment of the variation of the inclinations on the side walls (2) and (6).

TABLE IV
VALUES OF I_ω ($x\ 10^8$) m^6 FOR THE VARIATION OF THE INCLINATION OF
WALLS (2), (3), (6) E (7)

θ_2	θ_6	$\theta_3 = 285^0$; $\theta_7 = 195^0$			$\theta_3 = 322.5^0$; $\theta_7 = 217.5^0$		
		curve 1	curve 2	curve 3	curve 1	curve 2	curve 3
15^0	165^0	1.221	0.502	104.968	1.967	0.821	168.500
30^0	150^0	1.017	0.424	87.208	1.645	0.696	140.643
45^0	135^0	0.697	0.295	59.561	1.136	0.486	96.917
60^0	120^0	0.359	0.156	30.615	0.580	0.251	49.378
75^0	105^0	0.102	0.046	8.662	0.151	0.068	12.849

θ_2	θ_6	$\theta_3 = 360^0$; $\theta_7 = 180^0$		
		curve 1	curve 2	curve 3
15^0	165^0	1.744	0.753	148.573
30^0	150^0	1.443	0.636	122.467
45^0	135^0	0.977	0.440	82.704
60^0	120^0	0.493	0.228	41.629
75^0	105^0	0.133	0.065	11.197

As for Figures 12 (b), (c) and (d), the graphs of variation I_ω are plotted to the detriment of the inclinations of the wall panels (2), (6), (3) and (7). A total of three mirrored inclination values for panels (3) and (7), being: $\theta_3 = \{285^o; 322.5^o; 360^o\}$ and $\theta_7 = \{195^o; 217.5^o; 180^o\}$ are also adopted. It is noteworthy that curves 1, 2 and 3 are assembled in a manner similar to item III (A). Thus, the following relationships are expressed for the dimensions of the walls: $b_1 = b_2 = b_3 = b_6 = b_7$, $b_4 = b_5 = b_8 = b_9$, $t = b_1.\eta_3$ and $b_4 = \eta_4.t$.

IV. NUMERICAL APPLICATIONS

In order to validate the generalized formulas (see items II A and II B), the modeling of metal double T reinforced concrete columns is carried out, via CMT and FEM by the ANSYS Release 11 Software. Thus, an inclination sub-case of the wall panels is used, already characterized in the literature. Finally, the vibration modes are used as a parameter for verifying the good operationalization of item II of this article.

A. Modeling of the metal double T column

The column with cross section is modeled by the ANSYS Release 11 software for the occurrence of double T with double symmetry, employing 100 meters in height and wall panels with the following dimensions: $b_1 = 3.45\ m$, $b_2 = b_6 = b_3 = b_7 = 1.725\ m$ $b_4 = b_5 = b_8 = b_9 = 1.00\ m$, thickness t = 0.15 m and walls orthogonal to each other. Figure 13 shows the geometry of such a metal column with the following properties: $E = 2.1\ x\ 10^8\ kN/m^2$, $\gamma_{steel} = 7.8\ x\ 10^3\ kN/m^3$ and $v = 0.3$, whereas, Figures 14 and 15 show the first modes of vibration. The quality of the FEM mesh used in ANSYS was 99.66%, with 470,738 nodes and 66,700 FE for the double T column without lintels. A total of 69,500 FE and 493,853 nodes were also used to model the braced column. The modeled column has lintels with a thickness e_L of 15 cm, and height $h_L =$

1.00 meter. The spacing of these lintels is 5.00 meters (from axis to axis).
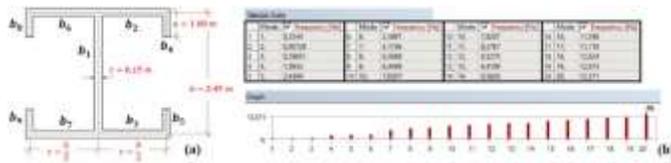
Fig. 13. Structural core metal column: (a) thin-walled section; and (b) vibration frequencies via software ANSYS 2019 Release 11, for the metal column without lintels.
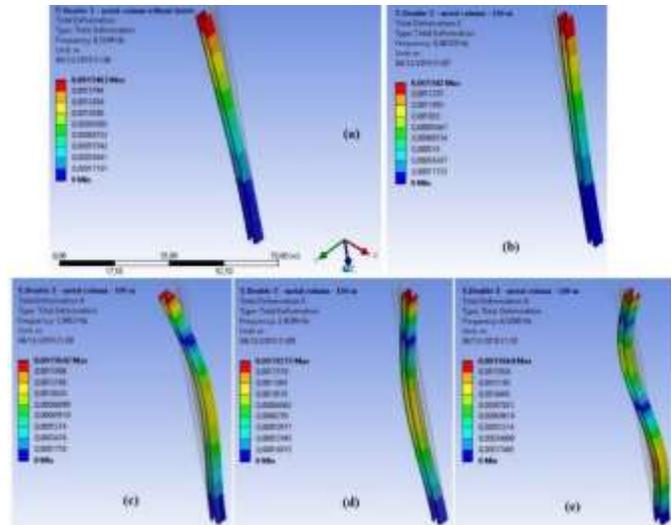
Fig. 14. Modes of vibration of the metal double T column without lintels via modeling by ANSYS: 1st mode in (a) x, (b) y; 2nd mode in (c) x, (d) y and (e) 3rd mode in y.
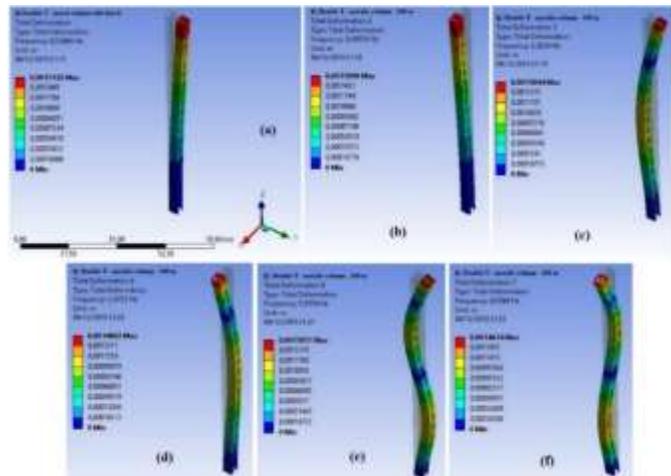
Fig. 15. Modes of vibration of the metal T column in double T bracing by lintels via modeling by ANSYS: 1st mode in (a) x, (b) y, 2nd mode in (c) x, (d) y, 3rd mode in (e) x and (f) y.

Table V shows the comparison of the first three modes of vibration as for flexure, and table V compares the terms of manual calculation and computer simulation via the ANSYS (see Figures 14 and 15). It is noteworthy that the manual calculation is performed for metal column without lintels.

Therefore, $s_j = 0$, whose analysis concludes an approximation of 4.4 % for the first mode to flexure vibration. Such approximation is due to the fact that the solution employed via CMT, see Melo & Barbosa (2020 a), is approximated by a finite number of terms of the power series that express the trigonometric and hyperbolic functions. Such approximations evidenced in Table V are due to the solution with 11 power series terms to solve the transcendental equation, using FEM mesh for modeling in the ANSYS, student version software. By increasing the number of terms in the series, there is the Mathcad's, outdated student version, workability, and the correct data processing does not occur. Even so, there is (with Table 5) an order of magnitude verification tool for simulations in commercial software. Usando: $\Delta(\%) = \frac{(f_{CMT} - f_{ANSYS})}{f_{CMT}} x100$.

TABLE V
COMPARISON OF THE FIRST THREE MODES OF VIBRATION TO FLEXURE, VIA COMPUTER MODELLING

Bracing	f	Manual calculation – via Table VI	Simulation via ANSYS	Δ (%)
without lintels $s_j = 0.0$	1st	$^1/_{1.3} \cdot (0.55959) \equiv 0.43045\ Hz$	0.40729 Hz	5.38
	2nd	$^2/_3 \cdot (3.50690) \equiv 2.33793\ Hz$	2.43940 Hz	4.34
	3rd	$^2/_3 \cdot (9.81960) \equiv 6.54640\ Hz$	6.30480 Hz	3.69
Horizontal lintels equally spaced by $h = 5.00\ m$ $(s_j = 8.07)$	1st	$0.40526\ Hz$	0.40918 Hz	0.97
	2nd	$^2/_3 \cdot (3.94602) \equiv 2.63068\ Hz$	2.47520 Hz	5.91
	3rd	$^2/_3 \cdot (10.47998) \equiv 6.98665\ Hz$	6.55640 Hz	4.35
			Average difference in percentage	4.11

Such weighting of the results obtained via CMT is postulated in Dziewolski (1964), where coefficient $\alpha = 1 / 1.5\ (\equiv 2 / 3)$ of adjustment for the vibration frequencies is proposed, in simple structures, through the CMT, applicable in this article for the 2nd and 3rd vibration modes. As for the complex structures, like the first vibration mode for activating more deformation energy, coefficient $\alpha = {}^1/_{1.3}$ is used as an adjustment. Still, Table VI presents the parameters used for the attainment of the frequencies via CMT, evidencing the theoretical basis for their generation in Melo & Barbosa (2020 a, b). It is noteworthy that, for $\lambda = H.\sqrt{s_1} \equiv 100\ m.\sqrt{0.006521} \equiv 8.07$ to use the tabulated value immediately closest, in this case, $\lambda = 10.0$ is the choice.

TABLE VI
COMPARISON OF THE FIRST THREE MODES OF VIBRATION TO FLEXURE, VIA COMPUTER MODELLING

$\lambda = H.\sqrt{s_j}$		Mode $i = 1$	Mode $i = 2$	Mode $i = 3$	Mode $i = 4$	Mode $i = 5$	Mode $i = 6$	Mode $i = 7$
	$\lambda_1\ [ADM]$	1.87510	4.69409	7.85483	9.08911	10.02092	11.68901	14.62618
	$\lambda_2\ [ADM]$	1.87510	4.69409	7.85483	9.08911	10.02092	11.68901	14.62618
0.0	$\omega_i^*\ [rad/s]$	3.51600	22.03448	61.69835	84.61192	105.97714	136.63295	213.92514
	$T_i^*\ [s]$	1.78703	0.28515	0.10184	0.07606	0.05929	0.04599	0.02937
	$f_i^*\ [Hz]$	**0.55959**	**3.50690**	**9.81960**	**13.46640**	**16.86790**	**21.74580**	**34.04724**
	$\lambda_1\ [ADM]$	2.89825	5.30895	8.29810	9.50762	10.32883	11.82274	14.57512
	$\lambda_2\ [ADM]$	0.94861	4.54807	7.83316	9.10466	9.95915	11.50118	14.31552
7.5	$\omega_i^*\ [rad/s]$	2.74930	24.14548	65.00038	86.56365	102.86640	135.97548	208.65043
	$T_i^*\ [s]$	0.43756	3.84290	10.34554	13.77790	16.37197	21.64033	33.21156
	$f_i^*\ [Hz]$	**2.89825**	**5.30895**	**8.29810**	**9.50762**	**10.32883**	**11.82274**	**14.57512**

$\lambda_1\,[ADM]$	3.25746	5.50391	8.42839	9.64266	10.43138	11.87014	14.61565
$\lambda_2\,[ADM]$	0.78169	4.50478	7.81267	9.10938	9.94051	11.44116	14.26945
10.0 $\omega_i^*\,[rad/s]$	2.54634	24.79389	65.84820	87.83870	103.69321	135.80821	208.55730
$T_i^*\,[s]$	2.46754	0.25342	0.09542	0.07153	0.06059	0.04627	0.03013
$f_i\,[Hz]$	**0.40526**	**3.94602**	**10.47998**	**13.98015**	**16.50437**	**21.61228**	**33.18951**

Figure 16 presents the change of the elastic line into the first modes of vibration for $s_j = 0$ (in the absence of lintel bracing) carrying out the analysis by CMT.
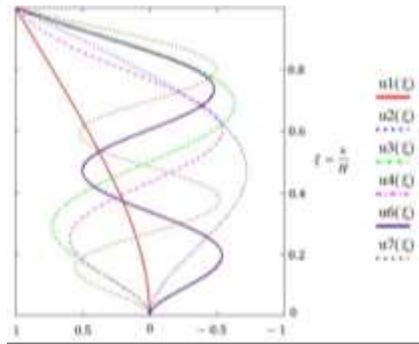
Fig. 16. First vibrations of the thin-walled column with fixed base and free top.

B. Modeling of the metal double T column

The column shown in item IV (A) is modeled using the ANSYS Release 11 software, adapting the cross section for the occurrence of double T with double symmetry, as well as using reinforced concrete with Young Module $= 52\,GPa$ and Poisson's coefficient $\nu = 0.2$. Thus, Figure 13 (a) shows the geometry of such a column, where the lintels are imposed with a thickness e_L of 25 cm, height h_L of 1.00 meter and are spaced (from axis to axis) by the distance h of 5.00 meters. As for Figures 17 and 18, the first modes of vibration of the column are presented without bracing and with locking promoted by the lintels, respectively. In the column without lintels, 167,498 nodes and 23,600 FE were used for modeling by ANSYS, obtaining a quality of 99.65% for the FE mesh. As for the braced column, 99.67% of the mesh quality was evidenced, with the use of 162,313 nodes and 22,560 finite elements.
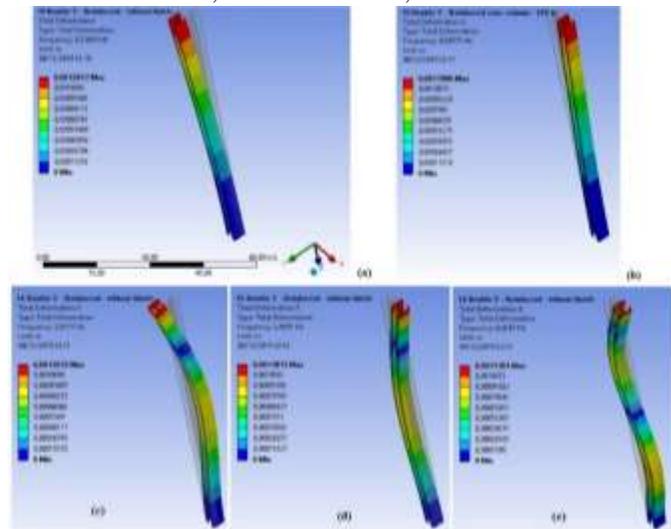
Fig. 17. Modes of vibration of the reinforced concrete double T column without lintels via modeling by ANSYS: (a) 1st mode of flexion around the x-axis, (b) 1st mode with flexion deformation around the y-axis, (c) 2nd mode of flexion around the x-axis, (d) 2nd mode of flexion around the y-axis (e) 3rd mode of flexion around the y-axis.

Table VII shows the comparison of the first three modes of vibration as for flexure in the reinforced concrete column, and table VII compares the terms of manual calculation and computer simulation via the ANSYS (see Figures 17 and 18). It is noteworthy to inform that, for $\lambda = H.\sqrt{s_1} \equiv 100\,m.\sqrt{0.006092} \equiv 7.81$, the tabulated value (see Table VI) immediately closest, in this case $\lambda = 7.5$ is the choice. In addition, the following weighting coefficients were used for the column braced by lintels: $\alpha = {}^2/_3$ for the first vibration mode, and $\alpha = {}^1/_2$ for the 2nd and 3rd vibration modes. As for the column without bracing, the same weighting coefficients were used as in the example provided in item IV (A). In conclusion, modeling via CMT resulted in an average approximation of 95.81% in relation to the ANSYS software.

TABLE VII
COMPARISON OF THE FIRST THREE MODES OF VIBRATION TO FLEXURE, VIA COMPUTER MODELLING

Bracing	f	Manual calculation – via Table VI	Simulation via ANSYS	Δ (%)
without lintels $s_j = 0.0$	1st	${}^1/_{1.3} \cdot (0.55959) \equiv 0.43045\ Hz$	0.40771 Hz	5.29
	2nd	${}^2/_3 \cdot (3.50690) \equiv 2.33793\ Hz$	2.45010 Hz	4.80
	3rd	${}^2/_3 \cdot (9.81960) \equiv 6.54640\ Hz$	6.42670 Hz	1.83
Horizontal lintels equally spaced by $h = 5.00\ m$ ($s_j = 7.81$)	1st	${}^2/_3 \cdot (0.43756) \equiv 0.33659\ Hz$	0.33652 Hz	0.02
	2nd	${}^1/_2 \cdot (3.84290) \equiv 1.92145\ Hz$	2.05130 Hz	6.76
	3rd	${}^1/_2 \cdot (10.34554) \equiv 5.17277\ Hz$	5.50520 Hz	6.43
			Average difference in percentage	4.19
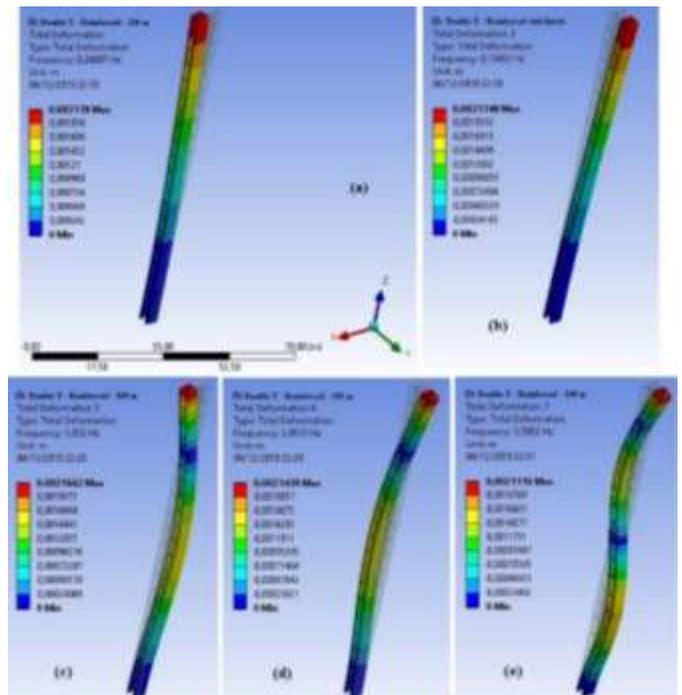
Fig. 18. Modes of vibration of the reinforced concrete double T column braced by lintels via modeling by ANSYS: (a) 1st mode with flexion deformation around the y-axis, (b) 1st mode with flexion deformation around the x-axis, (c) 2nd flexion mode around the y-axis, (d) 2nd flexion mode

around the x axis and (e) 3rd flexion mode on the x-axis.

V. CONCLUSION

In this paper, the Generalization of Wall Panels Theory (GWPT) is carried out following the nomenclature presented in Vlassov (1962) and the equation of the walls by generic trigonometric formulation. The aforementioned formulation is operationalized through the incidence of the referred wall panels, presenting the geometric properties of the column in structural core format, regarding the flexure-pill phenomenon. Still, in the wall panel theory, the contribution of the modeling of bracing lintels via Maney equations (equilibrium equations for hyperstatic structures from the perspective of the displacement method) is carried out. The practical motivation for such an analysis, GWPT, is to provide a design tool for bridges with structural model in beams, and that the structural engineer can add economy to the project by merely inclining the walls that form the structural core-shaped s.

The analysis of the optimized inclination of the wall panels of the column in structural core is done for straight bridges and more precisely in item III (B). Three scenarios of relative positioning of panels (2) and (3) are analyzed, in which the inclination of wall (3) is kept fixed at the following angles: 285°; 322.5^o and 360°, respectively per scenario. As for the double T core, the inclinations of the walls (2) - (6) and (3) - (7) are optimized, considering as variation: θ_2 from 15^0 to 75^0 with the increment of 15 degrees, $\theta_3 = 285^0$; 322.5^0; 360^0, θ_6 and θ_7 symmetrical to angles θ_2 and θ_3, as shown in Figure 13 (a). In the analysis of the inclination of the wall panels, the objective is the variation of the sectoral inertia I_ω and consequent bimoment, providing tools for the structural engineer to add economy to the project with the mere inclination of the lateral walls of the column in structural core. Thus, promoting the reduction of the internal forces, of which it is relevant to mention the bimomento.

Moreover, it is proposed to extend the analysis of the panels, which postulation is found in Melo & Barbosa (2020 a) for massive or thin-walled closed cross-sections. The equation of the dynamic analysis in the open section columns is carried out in this article with the appropriate formulation generalized by the generic inclination of the wall panels. With the thin-walled sections open, the flexural torsion phenomenon is activated and, therefore, the structure stiffness is partitioned into two matrices, namely [J] the structural core stiffness matrix itself and [S] for lintels that promote bracing. For such dynamic treatment of the open section, the decoupling flowchart of this differential equation system is postulated. The vibration modes for metal columns are also analyzed, comparing manual processing via continuous media technique with FEM modeling through ANSYS Release 11 through the appropriate modal analysis tool. Finally, the validation of the generalized formulations is presented (see items II A and II B), in addition to the dynamic modeling via CMT and by ANSYS Release 11 for metal double T reinforced concrete columns, verifying 4.11 % and 4.19 %, respectively, in the first three modes of vibration.

APPENDIX

with: $\Delta_{1P} = \left(2.\omega_{pc_{f_1}} - \omega_{pc_P}\right)$; $\Delta_{P1} = \left(2.\omega_{pc_P} - \omega_{pc_{f_1}}\right)$; $\Delta_{12} = \left(2.\omega_{pc_{f_1}} - \omega_{pc_{f_2}}\right)$; $\Delta_{86} = \left(2.\omega_{pc_{f_8}} + \omega_{pc_{f_6}}\right)$;

$\Delta_{21} = \left(2.\omega_{pc_{f_2}} - \omega_{pc_{f_1}}\right)$; $\Delta_{P3} = \left(2.\omega_{pc_P} - \omega_{pc_{f_3}}\right)$; $\Delta_{3P} = \left(2.\omega_{pc_{f_3}} - \omega_{pc_P}\right)$; $\Delta_{79} = \left(2.\omega_{pc_{f_7}} + \omega_{pc_{f_9}}\right)$; $\Delta_{P7} = \left(2.\omega_{pc_P} + \omega_{pc_{f_7}}\right)$;

$\Delta_{24} = \left(2.\omega_{pc_{f_2}} + \omega_{pc_{f_4}}\right)$; $\Delta_{42} = \left(2.\omega_{pc_{f_4}} + \omega_{pc_{f_2}}\right)$; $\Delta_{35} = \left(2.\omega_{pc_{f_3}} + \omega_{pc_{f_5}}\right)$; $\Delta_{97} = \left(2.\omega_{pc_{f_9}} + \omega_{pc_{f_7}}\right)$; $\Delta_{7P} = \left(2.\omega_{pc_{f_7}} + \omega_{pc_P}\right)$;

$\Delta_{53} = \left(2.\omega_{pc_{f_5}} + \omega_{pc_{f_3}}\right)$; $\Delta_{16} = \left(2.\omega_{pc_{f_1}} + \omega_{pc_{f_6}}\right)$; $\Delta_{61} = \left(2.\omega_{pc_{f_6}} + \omega_{pc_{f_1}}\right)$; $\Delta_{68} = \left(2.\omega_{pc_{f_6}} + \omega_{pc_{f_8}}\right)$,

where: $\Delta\omega_{pc_{f_1}} = -b_1.\left(d_y.\cos\theta_1 + d_z.\sin\theta_1\right)$; $\Delta\omega_{pc_{f_3}} = -b_3.\left(d_y.\cos\theta_3 + d_z.\sin\theta_3\right)$;

$\Delta\omega_{pc_{f_2}} = -b_2.\left(d_y.\cos\theta_2 + d_z.\sin\theta_2\right) + b_1.b_2.\sin(\theta_1 - \theta_2)$;

$\Delta\omega_{pc_{f_5}} = -b_5.\left(d_y.\cos\theta_5 + d_z.\sin\theta_5\right) + b_3.b_5.\sin(\theta_3 - \theta_5)$;

$\Delta\omega_{pc_{f_4}} = -b_4.\left(d_y.\cos\theta_4 + d_z.\sin\theta_4\right) + b_1.b_4.\sin(\theta_1 - \theta_4) + b_2.b_4.\sin(\theta_2 - \theta_4)$; $\Delta\omega_{pc_{f_7}} = -b_7.\left(d_y.\cos\theta_7 + d_z.\sin\theta_7\right)$;

$\Delta\omega_{pc_{f_6}} = -b_6.\left(d_y.\cos\theta_6 + d_z.\sin\theta_6\right) + b_1.b_6.\sin(\theta_1 - \theta_6)$;

$\Delta\omega_{pc_{f_9}} = -b_9.\left(d_y.\cos\theta_9 + d_z.\sin\theta_9\right) + b_7.b_9.\sin(\theta_7 - \theta_9)$;

$\Delta\omega_{pc_{f_8}} = -b_8.\left(d_y.\cos\theta_8 + d_z.\sin\theta_8\right) + b_1.b_8.\sin(\theta_1 - \theta_8) + b_6.b_8.\sin(\theta_6 - \theta_8)$,

with: $\omega_{pc_P} = d_y.d_z$; $\omega_{pc_{f_1}} = \omega_{pc_P} + \Delta\omega_{pc_{f_1}}$; $\omega_{pc_{f_2}} = \omega_{pc_{f_1}} + \Delta\omega_{pc_{f_2}}$;

$\omega_{pc_{f_3}} = \omega_{pc_P} + \Delta\omega_{pc_{f_3}}$; $\omega_{pc_{f_7}} = \omega_{pc_P} + \Delta\omega_{pc_{f_7}}$;

$\omega_{pc_{f_4}} = \omega_{pc_{f_2}} + \Delta\omega_{pc_{f_4}}$; $\omega_{pc_{f_5}} = \omega_{pc_{f_3}} + \Delta\omega_{pc_{f_5}}$; $\omega_{pc_{f_6}} = \omega_{pc_{f_1}} + \Delta\omega_{pc_{f_6}}$; $\omega_{pc_{f_8}} = \omega_{pc_{f_6}} + \Delta\omega_{pc_{f_8}}$; $\omega_{pc_{f_9}} = \omega_{pc_{f_7}} + \Delta\omega_{pc_{f_9}}$.

$$d_z = \frac{-t}{I_z}.\int_s \omega_p.y \; ds$$

$$\equiv \frac{-t}{I_z}.\left\{\frac{b_2}{6}.\Delta\omega_2.(y_1 + 2.y_2) + \frac{b_4}{6}.\Delta\omega_2.(2.y_2 + y_4)\right.$$
$$+ \frac{b_4}{6}.(\Delta\omega_2 + \Delta\omega_4).(y_2 + 2.y_4)$$
$$+ \frac{b_5}{6}.\Delta\omega_5.(y_3 + 2.y_5) + \frac{b_6}{6}.\Delta\omega_6.(y_1 + 2.y_6)$$
$$+ \frac{b_8}{6}.\Delta\omega_6.(2.y_6 + y_8)$$
$$+ \frac{b_8}{6}.(\Delta\omega_6 + \Delta\omega_8).(y_6 + 2.y_8)$$
$$\left. + \frac{b_9}{6}.\Delta\omega_9.(y_7 + 2.y_9)\right\}$$

$$d_y = \frac{t}{I_y}.\int_s \omega_p.z \; ds =$$

$$\equiv \frac{t}{I_z} \cdot \left\{ \frac{d_2}{6} \cdot \Delta\omega_{2a} \cdot z_1 + \frac{(b_2 - d_2)}{6} \cdot z_2 \cdot (\Delta\omega_{2a} + 2.\Delta\omega_2) \right.$$

$$+ \frac{b_4}{6} \cdot \Delta\omega_2 \cdot (2.z_2 + z_4)$$

$$+ \frac{b_4}{6} \cdot (\Delta\omega_2 + \Delta\omega_4) \cdot (z_2 + 2.z_4)$$

$$+ \frac{b_5}{6} \cdot \Delta\omega_5 \cdot (z_3 + 2.z_5) + \frac{b_6}{6} \cdot \Delta\omega_6 \cdot (z_1 + 2.z_6)$$

$$+ \frac{b_8}{6} \cdot \Delta\omega_6 \cdot (2.z_6 + z_8)$$

$$+ \frac{b_8}{6} \cdot (\Delta\omega_6 + \Delta\omega_8) \cdot (z_6 + 2.z_8)$$

$$\left. + \frac{b_9}{6} \cdot \Delta\omega_9 \cdot (z_7 + 2.z_9) \right\} \qquad if\ b_{CG_z} \geq 0$$

$$\equiv \frac{t}{I_z} \cdot \left\{ \frac{b_2}{6} \cdot \Delta\omega_2 \cdot (z_1 + 2.z_2) + \frac{b_4}{6} \cdot \Delta\omega_2 \cdot (2.z_2 + z_4) \right.$$

$$+ \frac{b_4}{6} \cdot (\Delta\omega_2 + \Delta\omega_4) \cdot (z_2 + 2.z_4)$$

$$+ \frac{b_5}{6} \cdot \Delta\omega_5 \cdot (z_3 + 2.z_5) + \frac{d_6}{6} \cdot z_6 \cdot (\Delta\omega_{6a} + 2.\Delta\omega_6)$$

$$+ \frac{(b_6 - d_6)}{6} \cdot \Delta\omega_{6a} \cdot z_1 + \frac{b_8}{6} \cdot \Delta\omega_6 \cdot (2.z_6 + z_8)$$

$$+ \frac{b_8}{6} \cdot (\Delta\omega_6 + \Delta\omega_8) \cdot (z_6 + 2.z_8)$$

$$\left. + \frac{b_9}{6} \cdot \Delta\omega_9 \cdot (z_7 + 2.z_9) \right\} \qquad if\ b_{CG_z} < 0$$

with: $d_2 = \dfrac{|z_1|.b_2}{|z_1| + |z_2|}$; $\ d_6 = \dfrac{|z_6|.b_6}{|z_1| + |z_6|}$; $\ \Delta\omega_{2a} = \dfrac{d_2}{b_2}.\Delta\omega_2$ and $\Delta\omega_{6a}$

$$= \left(1 - \frac{d_6}{b_6}\right).\Delta\omega_6;$$

$$\Delta\omega_1 = \Delta\omega_3 = \Delta\omega_7 = 0;\ \Delta\omega_2 = b_1.b_2.\sin(\theta_1 - \theta_2);$$

$$\Delta\omega_5 = b_3.b_5.\sin(\theta_3 - \theta_5);\ \Delta\omega_6 = b_1.b_6.\sin(\theta_1 - \theta_6);$$

$$\Delta\omega_4 = -b_1.b_4.\sin(\theta_4 - \theta_1) - b_2.b_4.\sin(\theta_4 - \theta_2);$$

$$\Delta\omega_8 = b_1.b_8.\sin(\theta_1 - \theta_8) + b_6.b_8.\sin(\theta_6 - \theta_8);$$

$$\Delta\omega_9 = b_7.b_9.\sin(\theta_7 - \theta_9);\ z_p = -b_{CG_z};\ \text{and}\ y_p = b_{CG_y}.$$

REFERENCES

[1] A. O. Guelfond, *Calcul des differences finies*. Paris: Dunod, 1963.

[2] B. S. Smith, B. S. Taranath, *Tall building structures: analysis and design*. New York: John Wiley, 1991.

[3] B. S. Smith, A. Coull, "The analysis of tall core-supported structures subject to torsion," *Proceedings of civil engineering*, 53, pp. 173–187, Fev. 1972.

[4] B. Z. Vlassov, *Piéces longues en voiles minces*. Paris: Eyrolles, 1962.

[5] C. A. Brebbia, A. J. Ferrante, *The finite element technique*. Rio Grande do Sul: Editora UFRGS, 1975.

[6] C. F. Kollbrunner, K. Brasler, *Torsion in structures*. Berlin: Spronger-verlag, 1969.

[7] D. D. Mori, J. Munaiar Neto, *Flexo torção: barras com seção aberta e paredes delgadas*. São Carlos: EESC/USP, 2017.

[8] E. Mancini. (1972). *Associação continua tridimensional de porticos e paredes com engastamento elástico* [Dissertation]. EESC/University of Sao Paulo, Brazil. Available: http://www.set.eesc.usp.br/static/media

/producao/1972ME_EddieMancini.pdf.

[9] F. A. Campanari, *Teoria das estruturas*. Vol. 2. Rio de Janeiro: Guanabara Dois, 1985..

[10] G. Dhatt, G. Touzot, G. Lefrançois, *Méthode des éléments finis*. Paris: Lavoisier, 2005.

[11] J. A. Barbosa. (1978). *Edifícios com paredes de secção aberta contraventadas por lintéis, sob carga lateral* [Dissertation]. EESC/University of Sao Paulo, Brazil. Available: http://www.set.eesc.usp.br/static/media/producao/1978M E_JairAlvesB arbos a.pdf.

[12] J. E. Laier. (1984). *Estudo do comportamento dinâmico de estruturas de edifícios altos pela técnica do meio contínuo* [Ph.D. Thesis]. EESC/University of Sao Paulo, Brazil.

[13] J. M. Biggs, *Introduction to structural dynamics*. New York: McGraw-Hill, 1964.

[14] K. A. Zalka, *Global structural analysis of buildings*. London: Taylor & Francis Group, 2000.

[15] M. Laredo, *Grands bâtiments: contreventements, dynamique des structures, calcul automatique*. Paris: Eyrolles, 1977.

[16] M. C. Stamato, *Associação continua de painéis de contraventamento*. São Carlos: EESC/USP, 1980.

[17] N. W. Murray, *Introduction to the theory of thin-walled structures*. Oxford: Oxford University Press, 1986.

[18] R. Dziewolski, "Étude théorique et experimentale d'une pouter en caisson asymétrique avec deux apêndices," *IABSE Congress report*, pp. 131–147, 1964.

[19] W. I. G. Melo. N. P. Barbosa, "Dynamic modeling of metal columns with open sections," *International Journal of Steel Structures*, 20, pp. 833–855, June. 2020 a.

[20] W. I. G. Melo. N. P. Barbosa, "Dynamics decoupling in reinforced concrete columns in structural core shape and applied to bridges," *International Journal of Advanced Engineering Research ans Science*, 7, pp. 48–58, Mai. 2020 b.

[21] W. K. Tso, "Shear walls coupled by cross wall," *Journal of Structural engineering*, 109, pp. 2010–2016, Ago. 1983.